

Analysis of Stabilization Circuits for Phase-Noise Reduction in Microwave Oscillators

Almudena Suárez, *Senior Member, IEEE*, and Franco Ramírez

Abstract—Two configurations for oscillator phase-noise reduction using stabilization circuits have been demonstrated in the literature. One of them is based on the self-injection of the oscillator signal, after it passes through a long delay line or a high-quality-factor resonator. The second one is a stabilization loop, containing a frequency discriminator. In this paper, an in-depth analytical comparison of these two configurations, respectively based on injection locking and phase-locking principles, is presented. Analytical expressions are provided for the variation of the steady-state solution and its phase noise versus the parameters of the feedback network. The expressions are rigorously validated with harmonic balance. Instabilities reported by other authors are investigated through bifurcation analysis. The new expressions enable a good understanding of the amplitude and frequency jumps and sharp phase-noise maxima obtained simulations and measurements versus the feedback parameters. A practical 5-GHz voltage-controlled oscillator has also been implemented, for validation purposes.

Index Terms—Describing function, feedback oscillator, fold-type bifurcation, phase noise, self-injected oscillator.

I. INTRODUCTION

SEVERAL authors [1]–[6] have presented techniques for phase-noise reduction in existing microwave oscillators using feedback. The proposed feedback loops contain either a long delay line or a high-quality-factor resonator, coupled to a short line. In [1], [2], a self-injection topology is used based on the connection of a circulator to the oscillator output. After passing through a long delay line or a high-quality-factor Q resonator, the signal is re-injected to the oscillator circuit, which reduces the autocorrelation of the phase noise. In [1], [2] the phase-noise reduction is explained as the result of the oscillator synchronization to the re-injected RF signal. A second configuration, initially proposed by Altman [3], is a stabilization loop, in which feedback is introduced into a voltage-controlled oscillator (VCO) using a frequency discriminator. This discriminator [3], [4], [6] converts the frequency fluctuations into baseband voltage fluctuations, which provide an error signal that readjusts the oscillator solution. Although the overall circuit is actually a free-running oscillator, the phase-noise reduction may be intuitively understood as the result of the oscillator phase locking to a stabilized signal. No comparison between the performances of these two configurations has been performed, in terms of stability or phase-noise reduction, and it is believed that it could be of interest for the designer.

Manuscript received July 6, 2004; revised March 16, 2005. This work was supported under Spanish CYCIT Project TIC2002-03748.

The authors are with the Communications Engineering Department, University of Cantabria, 39005 Santander, Spain (e-mail: suarez@unican.es).

Digital Object Identifier 10.1109/TMTT.2005.854182

Although these configurations have been experimentally verified [1]–[5], there are few circuit-level analyses of their behavior versus the feedback-loop parameters. In the case of the self-injection topology, the stable operation ranges have been analytically determined [1], [2] neglecting the deviation of the oscillator amplitude and frequency from the free-running values. When compared with time-domain simulations, the obtained expressions fail to accurately predict the stability ranges. An analytical formulation [1], [2] has also been presented for the variation of the phase-noise spectral density. It gives explanation for the reduction of this spectral density versus the time delay. Again, the deviation of the oscillator solution from the free-running values is not taken into account. On the other hand, commercial harmonic-balance (HB) tools enable an accurate simulation of the steady-state solution and its phase noise. However, convergence difficulties and jumps are obtained for some values of the feedback elements, which prevent the tracing of the entire solution paths. Sharp phase-noise maxima of high magnitude are also observed when these elements are varied. The convergence difficulties and the reported unstable behavior demand an exhaustive investigation through bifurcation-analysis techniques [7], which, to our knowledge, has not yet been tackled.

In this study, an in-depth analytical study is carried out of the stability and phase noise of self-injected oscillators and stabilization loops using frequency discriminators. The analytical approach is different from that of [1] and [2] and takes into account the variations of the oscillation amplitude and frequency versus the feedback elements, which was proposed as a future research line in [2]. The main objective is the understanding of the instability phenomena reported by other authors and the influence of the feedback elements on the phase-noise behavior. The expressions are initially derived using a describing-function model for the nonlinear elements. However, the general application to practical oscillator circuits will require noise-analysis techniques based on harmonic balance, like the carrier-modulation [8], [9] and conversion-matrix approaches [9]–[11]. The qualitative agreement with the general behavior predicted by the new analytical formulation will be verified through the application of the two feedback techniques to a MESFET-based VCO at 5 GHz.

The paper is organized as follows. In Section II, the new analytical formulation for the self-injected oscillator is presented, considering, as in [2], the cases of a long delay line and high- Q resonator in the circulator loop. In Section III, an analytical formulation for the stabilization loop, containing a frequency discriminator, is presented and compared with that of the self-injected oscillator. In Section IV, the two techniques are applied to a VCO at 5 GHz, which has been manufactured and measured.

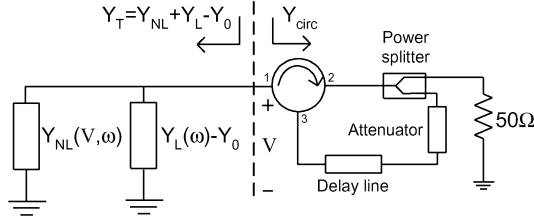


Fig. 1. Self-injected oscillator. The output load has been replaced with the circulator and delay line.

II. SELF-INJECTION TOPOLOGY FOR PHASE-NOISE REDUCTION

A. Steady-State Solution

In this section, a describing-function analysis of the oscillator circuit will be carried out. The free-running oscillator is modeled with the parallel connection of a nonlinear block, with the admittance $Y_N(V, \omega)$, and a linear block $Y_L(\omega)$. The steady-state equation is $Y_T(V, \omega) = Y_N(V, \omega) + Y_L(\omega) = 0$. Now, the self-injection topology of Fig. 1 is considered. In this topology, the oscillator output is connected to the circulator Port 1. After passing through an attenuator and a delay line (or an attenuator and a high- Q resonator), the signal is reinjected into the oscillator circuit through the circulator Port 3. From the oscillator viewpoint, the reflection structure basically operates as a load, with the reflection coefficient Γ . Taking this into account, the new steady-state equations are given by:

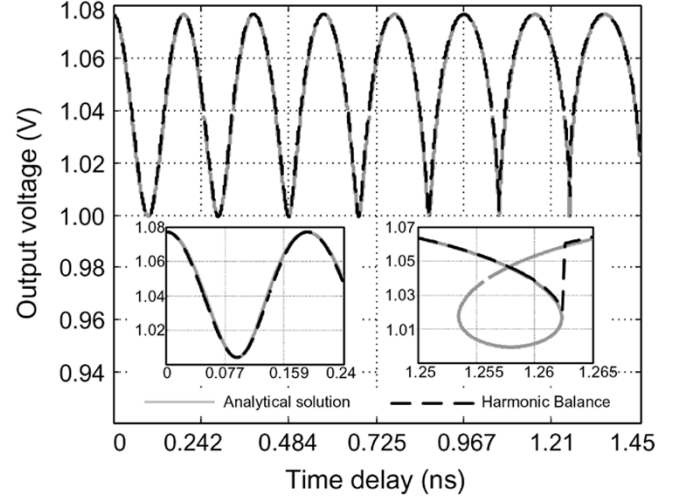
$$Y'_T(V, \omega) = Y_T(V, \omega) - Y_o + Y_{circ}(\omega) = 0 \quad (1)$$

with $Y_{circ} = Y_o(1 + \Gamma)/(1 - \Gamma)$ and Y_o the characteristic admittance. To avoid a big perturbation of the oscillator solution, high attenuation is usually introduced between Ports 2 and 3 of the circulator, so, in general, it will be possible to expand Y_{circ} in a first-order Taylor series about $\Gamma = 0$, which provides $Y_{circ} \cong Y_o(1 - 2\Gamma)$.

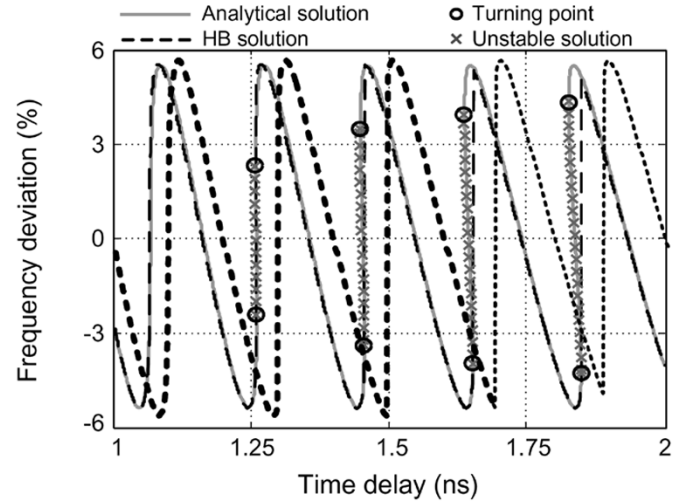
The case of a long delay line of electrical length θ , plus an attenuator, will initially be considered. The total loop attenuation will be given by A_L dB. Then, the reflection coefficient may be expressed: $\Gamma = 10^{-A_L/20} e^{-j\theta} = \rho e^{-j\omega\Delta T}$, where the modulus of the reflection coefficient and the time delay ΔT have been explicitly introduced. Substituting this into Y_{circ} and splitting (1) into real and imaginary parts, the following system is obtained:

$$\begin{aligned} G'_T &= G_T(V, \omega) - 2\rho Y_o \cos(\omega\Delta T) \\ &\cong G_{vo}(V - V_o) + G_{\omega o}(\omega - \omega_o) - 2\rho Y_o \cos(\omega\Delta T) \\ &= 0 \\ B'_T &= B_T(V, \omega) + 2\rho Y_o \sin(\omega\Delta T) \\ &\cong B_{vo}(V - V_o) + B_{\omega o}(\omega - \omega_o) + 2\rho Y_o \sin(\omega\Delta T) \\ &= 0 \end{aligned} \quad (2)$$

where the admittance function $Y_T = G_T + jB_T$ has been expanded in a first-order Taylor series about the free-running oscillator solution. The subindices indicate derivatives with respect to the corresponding variables. System (2) provides the variation of the self-injected oscillator solution, in terms of its amplitude and frequency, versus the time delay ΔT . The linearization about the free-running oscillation will be valid for high A_L ,



(a)



(b)

Fig. 2. Parallel-topology oscillator, based on a cubic nonlinearity $i = av + bv^3$, with $a = -0.037$ A/V and $b = 0.021$ A/V³. The linear-element values are $C = 0.715$ pF and $L = 1.328$ nH. Variation of the oscillator solution versus the time delay ΔT . (a) Oscillation amplitude. Comparison between the results obtained with (2) and using HB with one harmonic component. (b) Frequency deviation from the free-running value. Comparison between the results obtained with (2) and using HB with one and fifteen harmonic components.

which is usually the case. For low A_L , the oscillator steady-state solution should be recalculated for each ΔT value, using the describing function.

The feedback action of the self-injection topology is evidenced by (2), as the reflected signal depends on the oscillation frequency. As will be shown, the dependence of both Y_T and Y_{circ} on ω will lead to complex multivalued curves, for large ΔT values. This kind of solution cannot be obtained when the electrical length θ , instead of the delay ΔT , is used as a parameter, as in previous works.

For illustration, the system (2) has been particularized to the case of a parallel-resonance oscillator with a cubic nonlinearity. The variation of the steady-state solution, in terms of V and ω , versus the time delay ΔT is shown in Fig. 2, for the attenuation value $A_L = 30$ dB. As can be seen, only small deviations from the free-running amplitude and frequency are obtained in the

entire ΔT interval, which confirms the validity of the linearization in (2). The curves are single-valued for relatively small ΔT . However, from a certain ΔT value, they start to exhibit points of infinite slope (or turning points [7]). The lower sections of these curves fold over themselves, giving rise to the loops that are shown in the inset of Fig. 2(a). As known from bifurcation theory [7], the turning points give rise to a qualitative variation of the solution stability. The solution jumps to a different section of the multivalued curve and a sudden change is observed in the oscillator amplitude and frequency.

The validity of (2) has been verified through comparison with HB simulations considering one and fifteen harmonic components. Commercial HB has been used, unable to pass through the turning points. Thus, jumps are obtained between different curve sections at the turning points predicted by (2) [see the inset of Fig. 2(a)]. The excellent agreement for one harmonic component [Fig. 2(a)] validates (2). As could be expected, for a higher number of harmonic components [Fig. 2(b)], some quantitative discrepancies exist between the curves, but the qualitative behavior is still well predicted.

To summarize, two main differences exist between (2) and the expressions provided in previous works [1], [2]. In (2) and (3), a general dependence $Y_T = G_T(V, \omega) + jB_T(V, \omega)$ is considered, which is the usual case in practical transistor oscillators. In contrast, the expressions in [1] and [2] are only valid for dependences of the form $Y_T = G_T(V) + jB_T(\omega)$. On the other hand, the expressions in [1] and [2] neglect the variation of the steady-state amplitude and frequency in self-injected conditions, with respect to the free-running values. In (2), the use of ΔT as the analysis parameter enables the calculation of each new oscillator solution. As will be shown, this variation must be taken into account for an accurate determination of the stable-operation ranges and for the investigation of the bifurcation phenomena delimiting these ranges. Note that, in order to take the line dispersive effects into account, the physical length l should be used as the parameter, as will be done in the case of the transistor-based VCO of Section IV.

B. Stability

As shown in [7] and [9], at turning points of the oscillator solution curve, versus a particular parameter, the Jacobian matrix associated with the oscillator admittance function $Y_T(V, \omega)$ becomes singular. In the case of a self-injected oscillator, the Jacobian matrix analyzed will be the one corresponding to $Y'_T(V, \omega)$, given by $[JY'_T(V, \omega)]$. As already seen, the oscillator solution is recalculated for every ΔT value, so the determinant $\det[JY'_T(V, \omega)]$ will vary versus this parameter. The determinant is given by

$$\begin{aligned} \det [JY'_T(\omega, \Delta T)] &= G_{vo}(B_{\omega o} + 2\rho Y_o \Delta T \cos(\omega \Delta T)) \\ &\quad - B_{vo}(G_{\omega o} + 2\rho Y_o \Delta T \sin(\omega \Delta T)) \\ &= \det[JY_T]_o + 2\rho Y_o \Delta T (G_{vo} \cos(\omega \Delta T) \\ &\quad - B_{vo} \sin(\omega \Delta T)) \end{aligned} \quad (3)$$

where $\det[JY_T]_0 = G_{vo}B_{\omega o} - G_{\omega o}B_{vo}$. According to [9], the oscillator is stable versus synchronous perturbations $\det[JY'_T(V, \omega)] > 0$ and unstable for $\det[JY'_T(V, \omega)] < 0$.

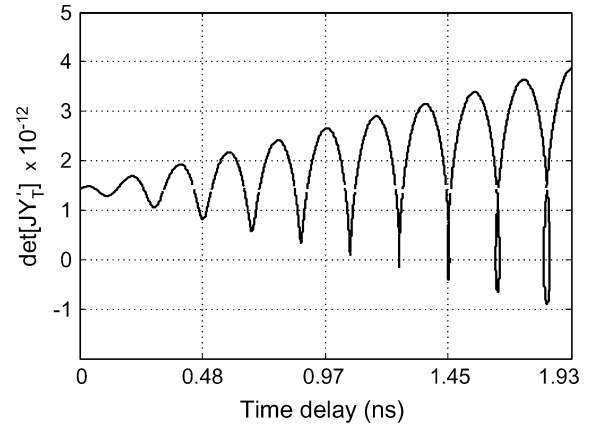


Fig. 3. Variation of $\det[JY'_T]$ versus the time delay ΔT . The turning point condition is $\det[JY'_T] = 0$.

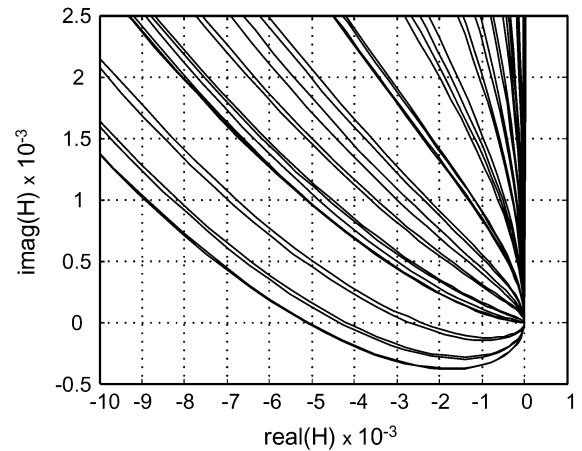


Fig. 4. Sequential stability analysis by means of the Nyquist plot, for different values of the time delay ΔT .

The solution will exhibit a turning point for $\det[JY'_T(V, \omega)] = 0$. For a direct calculation of the entire set of turning points, the system composed of (2) and (3) must be solved in terms of ΔT . Note that, for a stable free-running oscillation, the condition $\det[JY_T]_o > 0$ will be fulfilled. Thus, turning points can only be obtained when the amplitude of the sinusoidal term in (3), which is directly proportional to ΔT , becomes comparable to $\det[JY_T]$.

Fig. 3 shows the variation of $\det[JY'_T(V, \omega)]$ versus ΔT for the cubic-nonlinearity oscillator. The difference between the maxima and minima of this determinant increases with ΔT , as gathered from (3). As can be observed, the determinant zeroes accurately predict the turning points. For the rigorous determination of the stable ranges, Nyquist stability plots [7] have been sequentially traced for all of the considered ΔT values, as shown in Fig. 4, where an expanded view about the origin is presented. Unstable behavior is obtained for the ΔT values for which the plot crosses the negative real semi-axis. In Fig. 2(b), points with unstable behavior, which are predicted by the Nyquist analysis, are indicated with crosses. The turning points (circles) have been directly calculated, solving (2) and (3). Each unstable section is located between two consecutive turning points. In contrast with the predictions of [1] and [2], these unstable sections are only obtained from a certain ΔT

value. The length of the unstable intervals increases with ΔT , as predicted by (3).

C. Phase-Noise Analysis

For the phase-noise analysis, a current noise source will be introduced in the oscillator circuit, connected in parallel between Y_L and Y_N . For simplicity, only noise about the oscillator carrier will be considered. The variations of the phase-noise spectral density versus the time delay ΔT will be analyzed through successive linearizations of the system equations about each steady-state oscillation. For an analytical derivation of the phase-noise spectrum, the carrier modulation $\Delta\omega(t)$ will be determined through application of the Kurokawa approach [9]. Note that, in spite of the self-injection loop, the circuit still behaves like a free running oscillator, as no external time reference is present, so the carrier-modulation analysis is applicable. This analysis is valid for low frequency offset from the carrier, so the phase-noise-reduction bandwidth cannot be determined. For bigger frequency offset, the matrix-conversion approach should be applied [8], [10]. However, the largest phase-noise reduction is expected close to the carrier [1], [2], so the carrier-modulation analysis will enable a good estimation of the oscillator performance. The equations of the perturbed oscillator are the following:

$$\begin{aligned} G_{vo}\Delta V(t) + G'_{\omega o} \frac{d\phi(t)}{dt} + \frac{B'_{\omega o}}{V_o} \frac{d\Delta V(t)}{dt} &= G_n(t) \\ B_{vo}\Delta V(t) + B'_{\omega o} \frac{d\phi(t)}{dt} - \frac{G'_{\omega o}}{V_o} \frac{d\Delta V(t)}{dt} &= B_n(t) \end{aligned} \quad (4)$$

where $G_n(t), B_n(t)$ are the conductance and susceptance, associated with the white-noise current, averaged over one period of the carrier frequency [9]. Assuming a noise frequency Ω and solving for $\Delta\omega$, the expression obtained for the phase-noise spectral density is shown in (5) at the bottom of this page. The above expression neglects the time variation of the amplitude perturbation ΔV . This variation is also neglected in the carrier modulation approach, which constitutes a multiharmonic generalization [7] of (5). Through (5), it is possible to obtain the evolution of the phase-noise spectral density at a particular frequency offset Ω_m versus the time delay ΔT . For a given ρ and fixed offset frequency Ω_m , provided the condition $2\rho Y_o \Delta T \gg \det[JY_T]$ is fulfilled, the minima of the noise spectral density will decrease as $-20 \log(\Delta T)$. These phase-noise minima correspond to the maxima of $G_{vo} \cos(\omega \Delta T) - B_{vo} \sin(\omega \Delta T)$, i.e., they are obtained from the condition $\tan(\omega \Delta T) = -B_{vo}/G_{vo}$, with $\cos(\omega \Delta T) > 0$. For $2\rho Y_o \Delta T \gg \det[JY_T]$, the maximum phase-noise reduction with respect to the free-running value tends to $\Delta S = 20 \log(2\rho Y_o \Delta T |Y_{TVo}| / \det[JY_T]) = -A_L + 20 \log(2Y_o \Delta T |Y_{TVo}| / \det[JY_T])$, with $Y_{TVo} =$

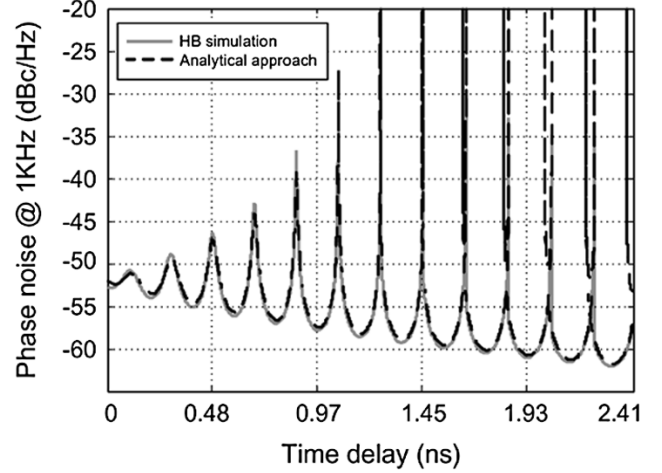


Fig. 5. Phase-noise variation versus the time delay ΔT at fixed frequency offset from the carrier $f_m = 1$ kHz. The analytical results are compared with commercial HB simulations, using the carrier modulation approach.

$(\partial Y_T)/(\partial V)|_o$. Larger reduction is obtained for smaller attenuation A_L . Taking (2) into account, it can easily be demonstrated that minimum frequency deviation, with respect to the free-running value ω_o , is obtained at the phase-noise minima, which is very convenient for the oscillator design. Fortunately, the points with minimum phase noise also lie on the stable sections of the solution curves.

The denominator of (5) agrees with $\det[JY'_T(V, \omega)]$ [see (3)], so divisions by zero are obtained at the turning points. The phase noise will tend to infinity at these points. It must be noted that the system linearization that is always used in phase-noise analysis is no longer valid in the neighborhood of the turning points, since the amplitude perturbation ΔV grows rapidly as these points are approached.

For illustration, (5) has been used for the phase-noise analysis of the parallel-topology oscillator. In Fig. 5, the phase-noise spectral density, at a fixed frequency offset $f_m = 1$ kHz, with $f_m = \Omega_m/2\pi$, has been traced versus the time delay ΔT . As previously discussed, the phase noise tends to infinity at the turning points of the solution curve. On the other hand, the phase-noise minima lie in the stable sections, as can be verified through comparison with Figs. 2 and 3. For validation, HB simulations using the carrier modulation approach [8] have been superimposed. An improvement of about 10 dB is obtained for the time delay $\Delta T = 2.33$ ns.

The variation of the steady-state solution and its phase-noise spectral density at $f_m = 1$ kHz have also been analyzed versus the bias voltage of a varactor diode for fixed time delay $\Delta T = 6.5$ ns (Fig. 6). The interest of this particular analysis comes from the fact that, in contrast with the line length, this parameter can be continuously varied in the experiment. As can be seen, turning points, delimiting the stability margins, are also

$$|\Delta\phi(\Omega)|^2 \cong \frac{|G_{vo}B_n(\Omega) - B_{vo}G_n(\Omega)|^2}{[\det[JY_T]_o + 2\rho Y_o \Delta T (G_{vo} \cos(\omega \Delta T) - B_{vo} \sin(\omega \Delta T))]^2 \Omega^2} \quad (5)$$

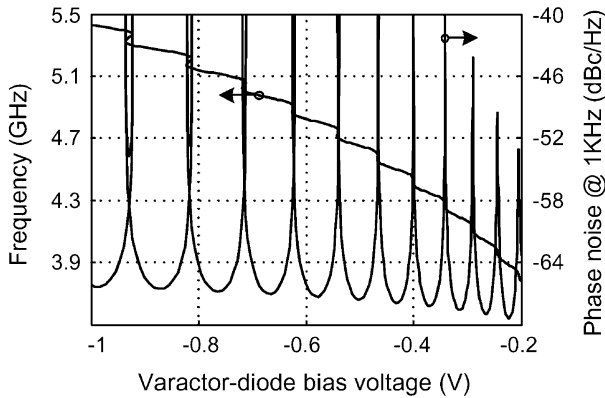


Fig. 6. Parallel-topology oscillator, with cubic nonlinearity. Variation of the steady-state solution, in terms of the oscillation frequency, versus the bias voltage of the varactor diode. The evolution of the phase-noise spectral density at fixed offset $f_m = 1$ kHz is superimposed.

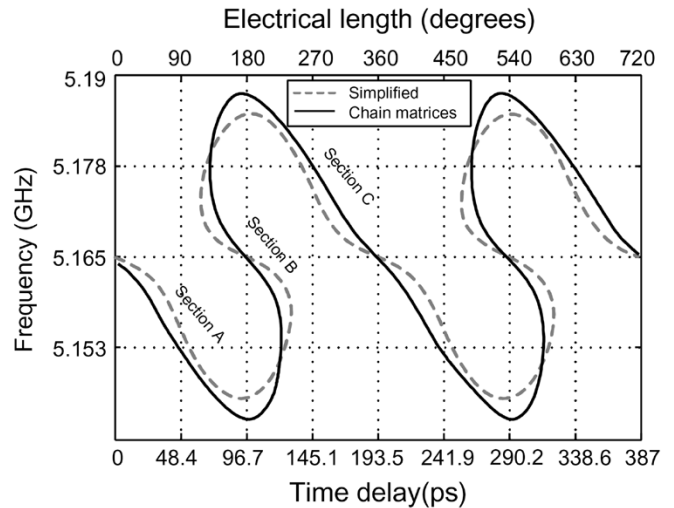
observed when this parameter is used. The phase-noise maxima are obtained at these turning points.

D. Use of Dielectric Resonators

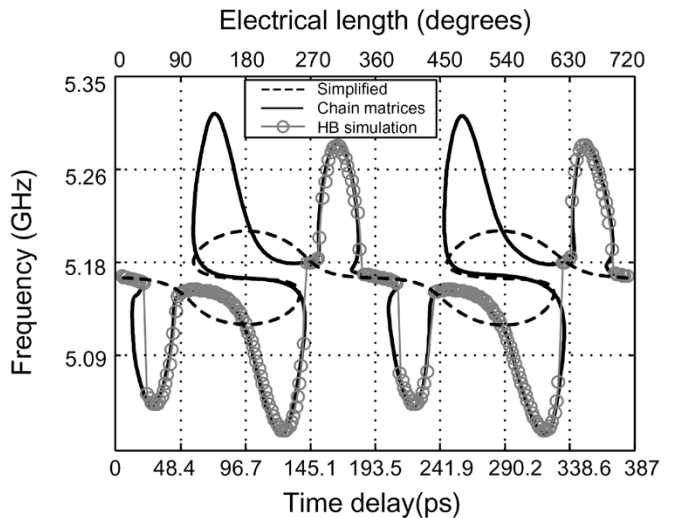
As shown in [1], [2], and [11], the use of a dielectric resonator increases the spectral purity of the re-injected signal. In the self-injected oscillator, the resonator is coupled to a transmission line in the circulator loop [2]. In former works [11], variations of the oscillation stability with the electric length θ of this line have been reported. Here, the steady-state oscillator solution and its stability and phase noise will be analyzed versus the line delay ΔT . Equation (1) will be used, which requires the calculation of Y_{circ} . Two different models for the coupled resonator will be used. The first model is the classical block model [11], consisting of a narrow bandpass filter $H(\omega)$, plus a phase shift $\theta = \omega\Delta T$. The second and more accurate model uses a chain matrix description for the transmission line and the resonator. Actually, the phase shift provided by the transmission line is only equal to its electrical length for matched terminations. With the second model, Y_{circ} is calculated from the multiplication of the chain matrices of the resonator and the delay line. The resulting matrix is transformed to a scattering matrix, which enables the determination of the input admittance Y_{circ} .

For illustration, a dielectric resonator, with $Q = 1000$ and resonance frequency $f_o = 5.16$ GHz, has been introduced in the self-injection loop of the parallel-topology oscillator. Fig. 7 shows a comparison between the analysis results in terms of the oscillation frequency when the two models are used. Two different attenuation values have been considered: $A_L = 30$ dB [Fig. 7(a)] and $A_L = 15$ dB [Fig. 7(b)]. There are discrepancies between the two, which increase as the attenuation is reduced.

As can be seen, there are some intervals with three coexisting solutions, delimited by turning points. For maximum rigor, the stable regions of the curves in Fig. 7(a) have been determined through sequential Nyquist analyses, as in the previous section, and through pole-zero identification techniques [12]. Fig. 8 shows the complex-conjugate poles closest to the imaginary axis, corresponding to the three coexisting solutions, for $\Delta T = 0.1$ ns. As can be seen, the solutions in Sections II-A and II-C are stable, while the solution in Section II-B is unstable. There



(a)



(b)

Fig. 7. Self-injected oscillator with a dielectric resonator in the circulator loop. Variation of the oscillation frequency versus the time delay ΔT . Comparison between the results obtained when using simplified and accurate coupled-resonator models, for two different values of the loop attenuation. (a) $A_L = 30$ dB. (b) $A_L = 15$ dB.

is also, for each of the three solutions, a pair of complex-conjugate poles on the imaginary axis at the oscillation frequency.

As already mentioned, for smaller attenuation A_L , greater discrepancy is obtained between the results obtained with the two coupled-resonator models [see Fig. 7(b)]. When a rigorous calculation of Y_{circ} is carried out, a second multivalued region is obtained, not predicted with the simplified expression. Fig. 7(b) shows a comparison between the results of the describing-function analysis and those obtained with commercial HB. The excellent agreement with the analytical predictions when using the accurate resonator model can be observed. With commercial HB, it is not possible to pass through the solution turning points, and a jump is obtained to a different curve section. Because the sections are very close, the discontinuity of the response might be difficult to note and a continuous curve may be wrongly assumed.

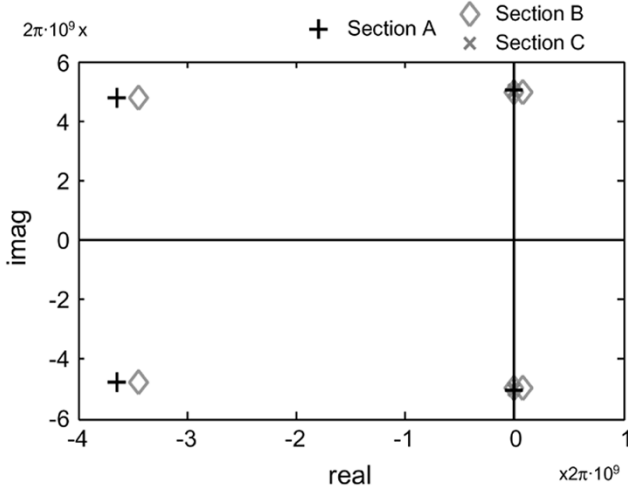


Fig. 8. Self-injected oscillator with dielectric resonator in the circulator loop. Application of the pole-zero identification technique [12] to the three solutions coexisting for the time delay $\Delta T = 0.1$ ns [Fig. 7(a)].

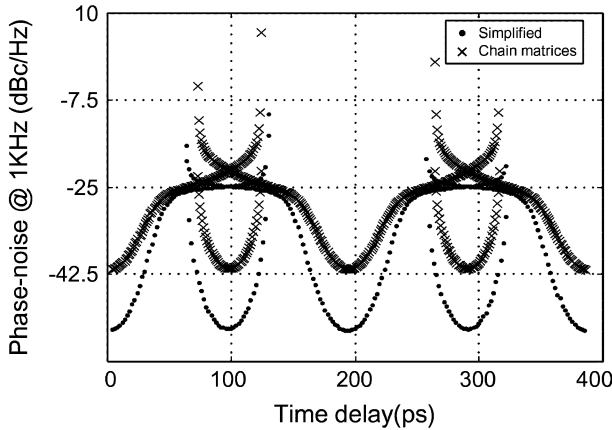


Fig. 9. Self-injected oscillator with dielectric resonator in the circulator loop. Variation versus the time delay ΔT of the phase-noise spectral density at $f_m = 1$ kHz. The attenuation value is $A_L = 30$ dB.

The variations of the phase-noise spectral density for the attenuation value $A_L = 30$ dB, at the constant frequency offset $f_m = 1$ kHz, are shown in Fig. 9. Compared with the use of the delay line, higher phase-noise reduction is achieved with the resonator. Again, the phase noise tends to infinity at the turning points of the solution curve, where the linearization is no longer valid.

III. STABILIZATION LOOP

In the feedback topology proposed in [3]–[6], phase-noise reduction is achieved with a stabilization loop containing a frequency discriminator. The loop operates as shown in Fig. 10. A fraction of the oscillator output signal is extracted through a coupler and is injected into a power divider. One of the divider outputs is delayed by means of a long transmission line. The two signals are introduced in a frequency mixer, acting as a phase comparator. The mixer output provides an error signal, which, after passing through a low-frequency amplifier, is introduced in a varactor diode. This corrects the oscillation frequency.

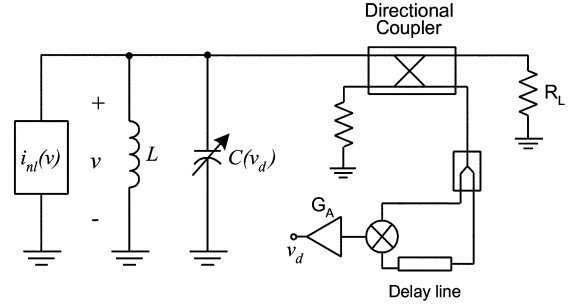


Fig. 10. Parallel-resonance oscillator with a stabilization loop containing a frequency discriminator. DC blocks and choke inductors are not represented.

The operation of the stabilization loop has been analytically studied here. The varactor capacitance varies according to $C(v) = C_{jo}/(1 - v_d/\varphi)^{1/2}$, where v_d is the low-frequency feedback voltage and φ is the built-in potential. For an approximate analysis, the steady-state solution is assumed $v(t) = V \cos(\omega t)$. Then, the two inputs of the frequency mixer will be: $v_1(t) = \gamma V \cos(\omega(t))$ and $v_2(t) = \gamma V \cos(\omega(t - \Delta T))$, where $\gamma = 10^{-A_L/20}$ and A_L is the total loop attenuation, including the power splitter. Then, the dc term at the varactor diode will be $V_{dc} = 1/2 G_A \gamma^2 V^2 \cos(\omega \Delta T)$, where G_A is the gain of the low-frequency amplifier.

To be able to carry out the analytical study, it will be assumed that the admittance Y_T can be linearized with respect to the feedback voltage $v_d(t)$, about the free-running value $v_d = 0$. Assuming a parallel resonance of the form in Fig. 10, the feedback-oscillator equations, with explicit dependence on ΔT , are the following:

$$\begin{aligned} G_{vo}(V - V_o) + G_{\omega o}(\omega - \omega_o) &= 0 \\ B_{vo}(V - V_o) + B_{\omega o}(\omega - \omega_o) + \frac{\partial B_T}{\partial v_d} \Big|_o K V_o^2 \cos(\omega \Delta T) &= 0 \end{aligned} \quad (6)$$

where $K = G_A \gamma^2 / 2$. Note that, for a simplified analysis, the dc term at the amplifier output has been approached $V_{dc} = K V_o^2 \cos(\omega \Delta T)$, where V_o is the free-running oscillation amplitude. The determinant of the Jacobian matrix associated with (6) is given by

$$\det [JY'_T] = \det [JY_T] - \alpha \Delta T \sin(\omega \Delta T) \quad (7)$$

with

$$\alpha = K V_o^2 G_{vo} \frac{\partial B_T}{\partial v_d} \Big|_o.$$

The above feedback configuration has been applied to the parallel-topology oscillator with cubic nonlinearity. Fig. 11 shows the variation of the oscillation frequency versus the time delay ΔT , for the amplifier gain $G_A = 20$ dB. As in the case of the self-injected topology, turning points are obtained from relatively large ΔT values. The turning points correspond to the zeroes of the determinant in (7). The stable and unstable sections have been distinguished through Nyquist stability analysis, obtaining unstable behavior between consecutive turning points, as shown in the inset of Fig. 11.

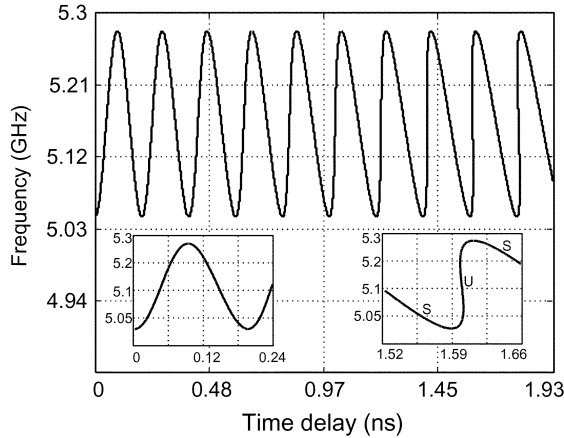


Fig. 11. Parallel-topology oscillator, with stabilization loop: variation of the oscillation frequency versus the time delay ΔT .

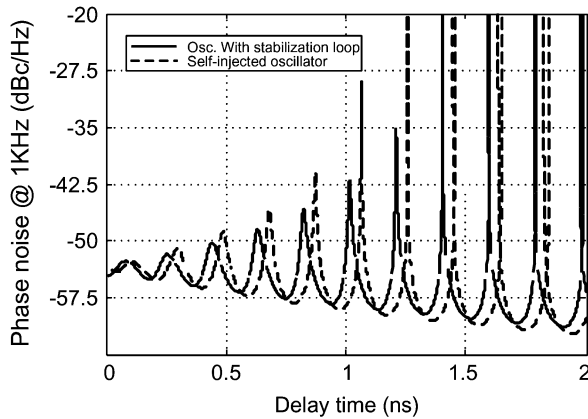


Fig. 12. Parallel-topology oscillator with stabilization loop. Variation of the phase-noise spectral density at $f_m = 1$ KHz, versus the time delay ΔT .

For the phase-noise analysis, only noise about the oscillator carrier has been introduced. Note that the objective of the work is the study of the loop action over the oscillator noise, so noise contributions from the external-loop elements are not considered. The carrier modulation is determined by differentiating the system (6), as has been done in (4), and solving for the perturbed frequency $\Delta\omega$. Close to the oscillator carrier, the phase-noise spectral density is approximately given by

$$|\Delta\phi(\Omega)|^2 = \frac{|G_{vo}B_n(\Omega) - B_{vo}G_n(\Omega)|^2}{(\det[JY_T] - \alpha\Delta T \sin(\omega\Delta T))^2\Omega^2} \quad (8)$$

where the denominator agrees with the determinant of the Jacobian matrix of (7), as expected in the quasi-stationary approach.

As in the case of the self-injected oscillator, the phase-noise spectral density, at a constant offset frequency Ω_m , varies in an oscillatory manner. In Fig. 12, this variation is analyzed at constant frequency offset $f_m = 1$ kHz. As soon as the product $\alpha\Delta T$ becomes dominant in the denominator of (8), the phase-noise minima decrease as $-20\log(\Delta T)$. For $\alpha\Delta T \gg \det[JY_T]$, the maximum reduction of the phase-noise spectral density with respect to the free-running value tends to $\Delta S = 20\log(\alpha\Delta T/\det[JY_T])$, with α being directly proportional to the loop gain K . Thus, the reduction increases with the loop gain. The phase-noise minima are obtained for $\sin(\omega\Delta T) = -1$, which, taking (6) into account, fortunately

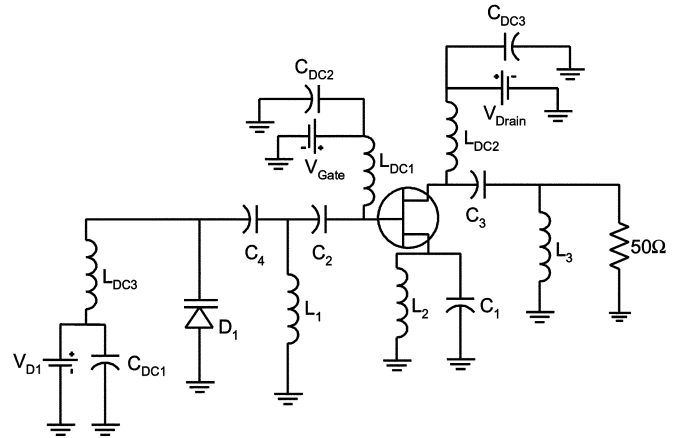


Fig. 13. Schematic of the 5-GHz VCO, to which the two feedback techniques for phase-noise reduction have been applied.

corresponds to a minimum deviation from the free-running oscillation frequency $\omega_o = 1/\sqrt{LC_{jo}}$. The phase-noise maxima, tending to infinity, are obtained at the denominator roots, which correspond to the turning points of (6). In Fig. 12, the results of the stabilization loop for $G_A = 20$ dB are compared with those obtained with the self-injection topology for $A_L = 20$ dB. In both cases, similar qualitative behavior is obtained, with a phase-noise improvement of more than 10 dB, with respect to the free-running oscillation.

IV. ANALYSIS AND EXPERIMENTAL CHARACTERIZATION OF A 5-GHz OSCILLATOR

When transistor-based oscillators are considered, with several noise sources, HB-based analysis is necessary for an accurate prediction of the oscillator response. In the carrier-modulation approach, the phase-noise variation will be inversely proportional to $\det[J(\bar{X}_o, \omega)]$, where J is the Jacobian matrix of the mixed-mode HB system [8] and \bar{X}_o is the vector containing the harmonic components of the state variables of the free-running oscillator solution. This Jacobian matrix involves derivatives with respect to the oscillation frequency that, in the determinant, will give rise to sinusoidal terms in $(n\omega\Delta T)$, where n is the harmonic index, having amplitude proportional to ΔT , in a similar way to (5) and (8). Thus, a qualitatively similar phase-noise variation may be expected.

The two different feedback techniques have been applied to a MESFET-based VCO, at 5 GHz, qualitatively comparing the analytical models with simulations and measurements. The oscillator schematic is shown in Fig. 13. For the simulation, the Angelov model has been used with four nonlinearities respectively given by the gate-to-source current i_{GS} and capacitance C_{GS} , the drain-to-source current i_{DS} , and the drain-to-gate current i_{GD} . The simulated VCO band was 4.6–5.4 GHz. In the measurements, the oscillation band was 4.7–5.30 GHz.

For the delay line, the substrate with $\epsilon_r = 10.2$ has been chosen. In this case, the physical length l of this line will be the analysis parameter, instead of the time delay. For each of the two configurations, the initial estimation of the required length and attenuation/gain values has been obtained using the analytical approaches and imposing a phase-noise reduction $\Delta S = 10$ dB.

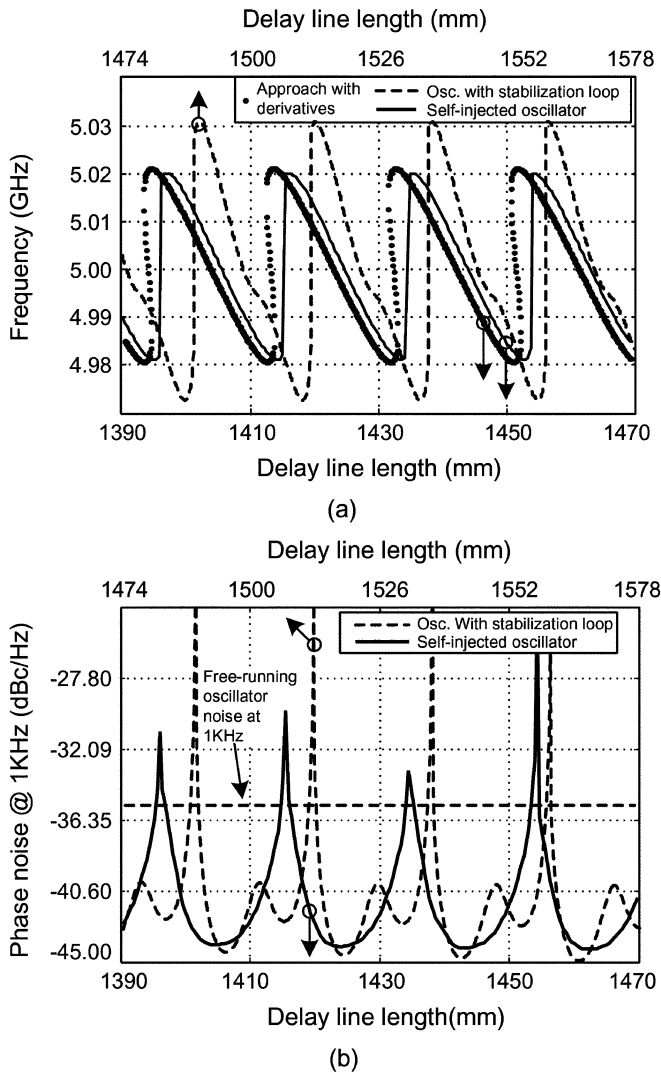


Fig. 14. VCO at 5 GHz with the two types of feedback. Self-injected topology, with $A_L = 20$ dB and $l_1 = 1.419$ m. Stabilization loop with discriminator, having amplifier gain $G_A = 10$ dB and $l_2 = 1.5$ m. (a) Variation of the oscillation frequency versus the physical line length. (b) Variation of the phase-noise spectral density at a constant offset frequency $f_m = 1$ kHz.

For the self-injected oscillator, the attenuation $A_L = 20$ dB and line length $l_1 = 1.419$ m have been chosen. For the stabilization loop, amplifier gain $G_A = 10$ dB and line length $l_2 = 1.5$ m are used. The line sections l_1 and l_2 have been implemented on two separate boards, with multiple line bends, to have a reasonably small size. The loss of the resulting structures has been taken into account in the estimations.

The solutions obtained with the two different feedback configurations are compared in Fig. 14(a), where the variation of the oscillation frequency with the line length has been represented. The solid- and dashed-line curves are HB simulations of the self-injected oscillator and stabilization loop with discriminator, respectively. As can be seen, slightly smaller frequency deviation is obtained with the self-injected oscillator [Fig. 14(a)]. For this topology, an estimation with the analytical model has also been superimposed. This has been obtained by introducing the derivatives Y_{vo} , $Y_{\omega o}$ of the free-running oscillator, at the cir-

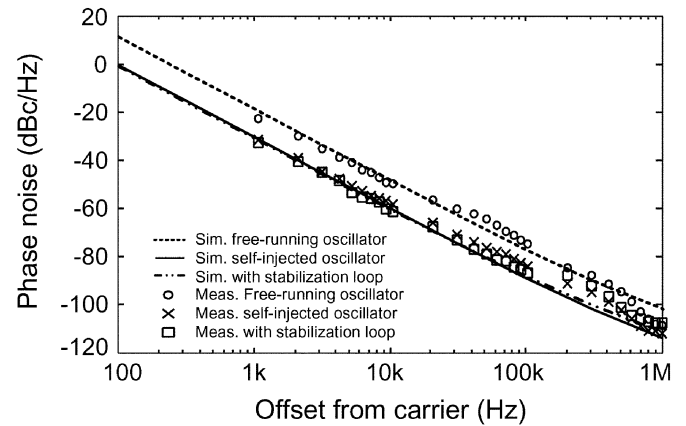


Fig. 15. VCO at 5 GHz. Comparison between the simulated and measured phase-noise spectra corresponding to the free-running oscillator, the self-injected oscillator, and the stabilization loop with discriminator, respectively.

culator connection node, into (2). The free-running-oscillator derivatives have been calculated in HB with the aid of an auxiliary generator, following the technique demonstrated in [13]. As can be seen, there is good qualitative agreement between the analytical model and HB. As expected, turning points are only obtained from sufficiently large values of the line length.

For the phase-noise analysis, several noise sources have been considered. A voltage noise source in series with the internal gate terminal accounts for the flicker noise. The spectral density of this source is $S_v = 9 \cdot 10^{-9} / \Omega$ V²/Hz. The shot noise is modeled with a current source of spectral density $2q i_{gs}$, where q is the electron charge, which is connected in parallel with the input Schottky diode. Thermal noise generators have also been added to all of the resistive elements. The phase-noise variation versus the delay-line length l , calculated with the carrier-modulation approach, at a constant offset frequency $f_m = 1$ kHz, is shown in Fig. 14(b). The results with the two different configurations can be compared. The sharp maxima at the turning points of the solution curves are in good qualitative agreement with the analytical models. Similar phase-noise reduction of about 9 dB is obtained with both configurations. The measured phase-noise spectrum confirming this phase-noise reduction is shown in Fig. 15. Simulations with the carrier-modulation [8], [9] and conversion-matrix approaches [10], [11] are also shown. The results with the two phase-noise analysis techniques are overlapped up to the frequency offset $f = 4$ MHz in the case of the self-injected oscillator and up to $f = 3$ MHz in the case of the stabilization loop. Although it is not presented here, the conversion-matrix approach shows a reduction of the phase-noise improvement as the frequency offset increases, in agreement with measurements.

Finally, the varactor bias voltage has also been used as a parameter. In contrast with the line length, this parameter can be continuously modified in the experiment, which enables a rigorous verification of the analysis results. The variation of the phase-noise spectral density using the self-injected configuration, at the three different offset frequencies 1, 10, and 100 kHz, respectively, is shown in Fig. 16. The experimental results have been superimposed.

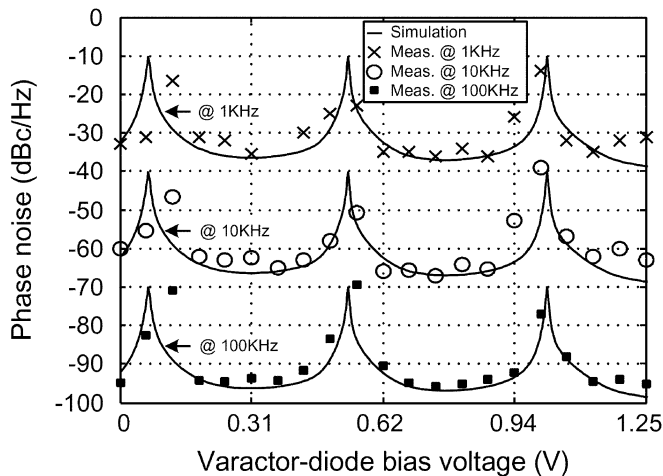


Fig. 16. Self-injected oscillator with $A_L = 20$ dB and $l_1 = 1.419$ m. Variation of phase-noise spectral density versus the bias voltage of the varactor diode for three different frequency offsets from the carrier. Measurements are superimposed.

V. CONCLUSION

In this paper, an exhaustive analysis of stabilization circuits for phase-noise reduction in microwave oscillators has been presented. Analytical expressions have been obtained, predicting the variation of the steady-state solution and its stability and phase noise versus the feedback-element values. Instability phenomena observed by other authors are explained using concepts from bifurcation theory. The analytical expressions have been rigorously verified through comparison with harmonic-balance simulations and the carrier-modulation approach for the phase-noise predictions. The feedback techniques have been applied to a 5-GHz VCO with very good experimental results.

ACKNOWLEDGMENT

The authors would like to thank J. Portilla, University of the Basque Country, Spain, for helpful advice and discussions.

REFERENCES

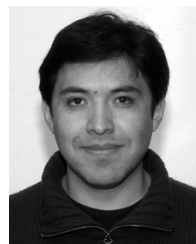
- [1] H. C. Chang, "Phase noise in self-injection-locked oscillators—Theory and experiment," *IEEE Trans. Microw. Theory Tech.*, vol. 51, no. 9, pp. 1994–1999, Sep. 2003.
- [2] —, "Stability analysis of self-injection-locked oscillators," *IEEE Trans. Microw. Theory Tech.*, vol. 51, no. 9, pp. 1989–1993, Sep. 2003.
- [3] J. L. Altman, "A technique for stabilizing microwave oscillators," *IEEE Trans. on Microw. Theory Tech.*, vol. MTT-2, no. 2, pp. 16–25, Jul. 1954.
- [4] U. L. Rohde and F. Hagemeyer, "Feedback technique improves oscillator phase noise," *Microw. RF*, vol. 37, no. 11, pp. 61–76, Nov. 1998.
- [5] C. E. Free and C. S. Aitchison, "Microwave oscillator control using a switched delay-line technique," in *IEEE MTT-S Int. Microwave Symp. Dig.*, Orlando, FL, May 1995, pp. 79–82.

- [6] C. McNeilage, E. N. Ivanov, P. R. Stockwell, and J. H. Searls, "Review of feedback and feedforward noise reduction techniques," in *Proc. IEEE Frequency Control Symp.*, Pasadena, CA, May 1998, pp. 146–155.
- [7] A. Suárez and R. Quéré, *Stability Analysis of Nonlinear Microwave Circuits*. Norwood, MA: Artech House, 2003.
- [8] V. Rizzoli, F. Mastri, and D. Masotti, "General noise analysis of nonlinear microwave circuits by the piecewise harmonic-balance technique," *IEEE Trans. Microw. Theory Tech.*, vol. 42, no. 5, pp. 807–819, May 1994.
- [9] K. Kurokawa, "Some basic characteristics of broadband negative resistance oscillator circuits," *Bell Syst. Tech. J.*, pp. 1937–1955, July–Aug. 1969.
- [10] J. C. Nallatamby, M. Prigent, J. C. Sarkissian, R. Quéré, and J. Obregón, "A new approach to nonlinear analysis of noise behavior of synchronized oscillators and analog-frequency dividers," *IEEE Trans. Microw. Theory Tech.*, vol. 46, no. 8, pp. 1168–1171, Aug. 1998.
- [11] J. C. Nallatamby, M. Prigent, M. Camiade, and J. Obregón, "Phase noise in oscillators—Leeson formula revisited," *IEEE Trans. Microwave Theory Tech.*, vol. 51, no. 4, pp. 1386–1394, Apr. 2003.
- [12] J. Jugo, J. Portilla, A. Anakabe, A. Suárez, and J. M. Collantes, "Closed-loop stability analysis of microwave amplifiers," *Electron. Lett.*, vol. 37, pp. 226–228, Feb. 2003.
- [13] F. Ramírez, E. de Cos, and A. Suárez, "Nonlinear analysis tools for the optimized design of harmonic-injection dividers," *IEEE Trans. Microw. Theory Tech.*, vol. 51, no. 6, pp. 1752–1762, Jun. 2003.



Almudena Suárez (M'96–SM'01) was born in Santander, Spain. She received the degree in electronic physics and the Ph.D. degree from the University of Cantabria, Santander, Spain, in 1987 and 1992, respectively, and the Ph.D. degree in electronics from the University of Limoges, Limoges, France, in 1993.

In 1987, she joined the Electronics Department, University of Cantabria, where she was involved with nonlinear simulation. From May 1990 to December 1992, she was on leave with the Institute de Recherche en Communications Optiques et Microondes (IRCOM), University of Limoges. Since 1993, she has been an Associate Professor (permanent since June 1995) with the University of Cantabria and a member of its Communications Engineering Department. She has coauthored the book *Stability Analysis of Microwave Circuits* (Norwell, MA: Artech House, 2003). Her areas of interest include the nonlinear design of microwave circuits and, especially, the nonlinear stability and phase-noise analysis and the investigation of chaotic regimes.



Franco Ramírez was born in Potosí, Bolivia. He received the electronic systems engineering degree from the Military School of Engineering "Mcal. Antonio José de Sucre," La Paz, Bolivia, and the Ph.D. degree from the University of Cantabria, Santander, Spain.

He joined the Communications Engineering Department, University of Cantabria, in 2001, and since then he has been involved in the development of computer-aided design techniques for the nonlinear analysis and design of microwave oscillators and analog

frequency dividers.